Deep Learning Model for Sea Surface Salinity Forecast in the Tropical Pacific Ocean during ENSO Events

Hao Chen[1], Xiaobin Yin[1], Xiaofeng Li[2,3], Qing Xu[1], and Yan Li[1]

[1]College of Marine Technology, Faculty of Information Science and Engineering, Ocean University of China, Qingdao, 266100.

[2]Key Laboratory of Ocean Circulation and Waves, Institute of Oceanology, Chinese Academy of Sciences, Qingdao, China.

[3]Center for Ocean Mega-Science, Chinese Academy of Sciences, Qingdao, China.

Corresponding author: X. Yin (yinxiaobin@ouc.edu.cn,)

Key Points:

- A data-driven model for tropical sea surface salinity (SSS) forecast using a SSS spatial-variation-dependent Loss function were proposed.
- The forecast results of deep learning model and remote sensing Climate Change Initiative (CCI) SSS and TAO SSS are highly consistent.
- The proposed SSS forecast model supports the forecast of large-scale oceanic and atmospheric phenomena associated with SSS.

Abstract

Sea surface salinity (SSS) in the eastern tropical Pacific Ocean significantly influences the process of sea-air interactions and exhibits a strong response during the analysis of the El Niño-Southern Oscillation (ENSO). Recently, satellites have provided long-term SSS data, and deep learning methods can achieve spatial-temporal forecasts. We developed a satellite-data-driven deep neural network (DNN) model to achieve reasonable forecasts of SSS fields associated with the ENSO using a series of past satellite SSS data. Our model achieved short- to medium-term forecasts for SSS from 6 to 96 days, with an error of less than 0.2 pss. Consistent with the Climate Change Initiative (CCI) SSS Anomaly (SSSA), the SSSA appears approximately 4 months earlier than the filtered Sea Surface Temperature Anomaly (SSTA) during ENSO events. Moreover, the SSSA index forecasted by the DNN also showed strong negative relationship with the Niño3.4 SST index during ENSO events.

Plain Language Summary

Salinity is a critical factor in driving ocean movement and studying climate change. The product, which combines three satellite missions, provides a SSS time series data with unprecedented accuracy over the 2010–2019 period, at a 50 km resolution. Deep learning methods can mine complicated rules deeply hidden in a large amount of SSS sequence and avoids modeling various complicated processes. A deep learning model is proposed for forecasting sea surface salinity and exploring the potential of forecasting large-scale ocean phenomena, which may be instructive for future studies of forecasts of oceanic phenomena associated with ocean parameters.

1 Introduction

Sea surface salinity (SSS) is an important indicator of the global water cycle. Like sea surface temperature (SST), SSS can affect the dynamic processes of the ocean by changing the density distribution of seawater, which plays an important role in sea-air interaction and global climate (Kido et al., 2021; Lagerloef et al., 2002; Du et al., 2019). With the launch of the Soil Moisture and Ocean Salinity (SMOS) satellite, the Soil Moisture Active and Passive(SMAP), and the Aquarius satellite, these satellites provide an opportunity for accurate and real-time SSS spatial-temporal monitoring (Boutin et al., 2018; Qin et al., 2020; Le Vine et al., 2007, Bao et al., 2019).

Sea surface salinity forecasting plays a very important role in monitoring the marine environment, studying the formation and circulation of water masses, and climate forecasting. Traditional statistical methods for predicting SSS include regression models (Urquhart et al., 2020; Qing et al., 2019). However, statistical methods do not describe the nonlinearity and randomness of SSS data very well, and the prediction error is large compared with machine learning methods. Different from statistical models, machine learning techniques mine information from historical SSS data to learn knowledge to make predictions. As a result, data-driven models rely more on SSS data than on knowledge in the field of ocean climate. In 2020, the LSTM-based SSS short-term prediction model was applied to the South China Sea, and the prediction error increased with the advanced prediction time, but it showed that deep learning has great potential in SSS prediction (Song et al., 2019). Deep learning technology combined with ocean satellite data has led to an increasingly diverse exploration of ocean spatial-temporal sequences (Li et al., 2020). Deep learning techniques such as long-term, short-term memory neural networks (LSTM) succeed at predicting ocean parameters such as sea surface temperature (SST), sea surface height anomaly, and sea ice parameters from days to years (Xiao et al., 2019; Shao et al., 2022; Ren et al., 2022). These studies demonstrate the performance of deep learning requires a deluge of satellite data. The abundance of satellite SST data provided an excellent opportunity to use deep learning to implement ENSO predictions for many years (Ham et al., 2019, Zheng et al., 2021).

Due to the limited high-quality data, deep learning techniques have not been well applied to satellite SSS fields forecast in previous studies. It was previously unimaginable to combine SSS fields with deep learning to forecast oceanic and climate phenomena. A Deep Neural network (DNN) with many hidden layers, derived from the artificial neural network (ANN) theory, is a valuable technique for modeling intricate interactions in huge databases (LeCun et al., 2015). The accumulation of satellite-derived SSS data from SMOS, SMAP, and Aquarius not only resolve mesoscale SSS variation and temporal scale but also allows for the development of advanced algorithms for exploring SSS time series data (Hasson et al., 2018; Kolodziejczyk et al., 2021; Huang et al., 2021; Lin et al., 2019; Melnichenko et al., 2021). ConvLSTM (Shi et al., 2015) converts fully connected LSTM weights to convolutions and realizes spatial-temporal series forecast. The ConvGRU (Shi et al., 2017) is modified according to ConvLSTM, and LSTM is converted into GRU for calculation.

In this study, we developed a DNN forecast model based on a deep learning model to forecast SSS fields in the eastern tropical Pacific Ocean for the first time. Furthermore, a SSS spatial-variation-dependent Loss function named cumulative square error (CSE) is designed to optimize our DNN model. The CSE improves the performance of the DNN SSS forecast model.

This paper is organized as follows. Data and study area are described in Section 2. The DNN-based method for SSS forecast and SSS pattern in ENSO events are described in Section 3. Section 4 presents experimental results. The conclusions are given in Section 5.

2 SSS Data

The daily SSS data used for this study is the Sea Surface Salinity Climate Change Initiative (CCI) global L4 SSS product from the European Space Agency (ESA) with a 25 km resolution, covering 2010-2019. The SMOS, Aquarius and SMAP measurements were combined for the first time to produce a level 4 (L4) meshed multitasking estimate of SSS. The CCI L4 SSS is more accurate than the SSS retrieved from a separate satellite sensor(Boutin et al., 2021).. The study area is in the eastern equatorial Pacific Ocean from 11°N to 11°N and 180°W to 100°W.

The seasonal variations of SSS are studied and associated with the daily SST from the Met Office's Operational Sea Surface Temperature and Sea Ice Analysis (OSTIA). The gridded SST fields had a spatial resolution of 0.05° before being resampled on the same 25km EASE 2.0 grid as the SSS fields. To evaluate the DNN SSS forecast, the daily SSS from the Tropical Atmosphere Ocean (TAO) mooring array at 110°W and 0°N is used.

3 Materials and Methods

3.1 DNN SSS forecast model

The DNN model (Figure 1a) is based on the deep learning model to forecast SSS fields. In semantic segmentation, neural networks with multiscale feature extraction are widely used (Krizhevsky et al., 2012) to achieve excellent remote sensing image classification. Our DNN model took advantage of this technology and replaced the fully connected layer with a convolutional layer. The DNN model consists of four stacked composite layers, and each of the four stacked composite layers has three ConvGRU layers and one convolutional layer with kernel sizes of 5×5, 3×3, 3×3, and 5×5, respectively. The three ConvGRU layers and the convolutional layer of each composite layer include 8, 16, 32, and 1 channel. The previous 10 SSS time steps are fed into the DNN (the input is a SSS sequence of shape 112×312×10), and values of all SSS are rescaled from [30.8, 36.9] to [−1, 1] pss. Rectified Linear Units (ReLU) are used to activate the ConvGRU layers of each composite layer (Nair et al., 2021). DNN with ReLU trains several times faster than their nonlinear counterparts. The tanh function is used for the last convolutional layer of the first three composite layers, while the last convolutional layer of the bottom composite layer uses the linear function.

The SSS are subsampled 3 times at the 2×2 average pooling and then fed to the corresponding composite layers at different stacking levels that process SSS at different spatial resolutions. This process ensures that the network computation volume is greatly reduced without losing the image's main features, and the network model's generalization ability is also improved. Except for the bottom composite layer, the output of each composite layer is up-sampled and fed to the lower stack level with a high-resolution composite layer. Because of the evolution of large-scale oceanic and climate variability, variations in SSS at different locations are highly correlated. Therefore, when forecasting the SSS at one location, we use the SSS sequences of other nearby locations within a wider area centered on the forecast location. As a result, we use a multiscale scheme to enlarge the receptive field of the composite layer. The receptive field of the composite layer can be enlarged before feeding the input information to it by subsampling the input maps through a 2×2 average pooling layer. ConvGRU and convolutional layers of each composite layer extract only local values within the receptive field, and the expansion of the receptive field takes full advantage of the values of nearby input locations. The resolution is then recovered by up-sampling the output. During the training stage, the SSS sequence was split into two datasets with a 3:2 proportion for training and validation. Based on mean value and the standard deviation (STD) distribution presented in Figure 1b and 1c, the SSS variability varies greatly in different regions but varies slowly within the same region. The MSE function did not effectively reduce the forecast error in regions with large variability. Therefore, we designed aa SSS spatial-variation-dependent Loss function that considers the grids in different regions (the improved result is given in Figure S1). The weights of our DNNs are updated with the loss function (CSE) calculated as (1).

$$\text{Loss} = \sum_{n=1(i,j)}^{N} (SSS_{result(i,j)} - SSS_{GT(i,j)})^2 \tag{1}$$

Where N is the total number of samples, $SSS_{GT(i,j)}$ is the CCI SSS (satellite SSS) at the last time step of the nth sample of the training or validation dataset at the grid (i, j) of the real area, and $SSS_{result(i,\,j)}$ is the forecast SSS at the same time step forecast result by the DNN.

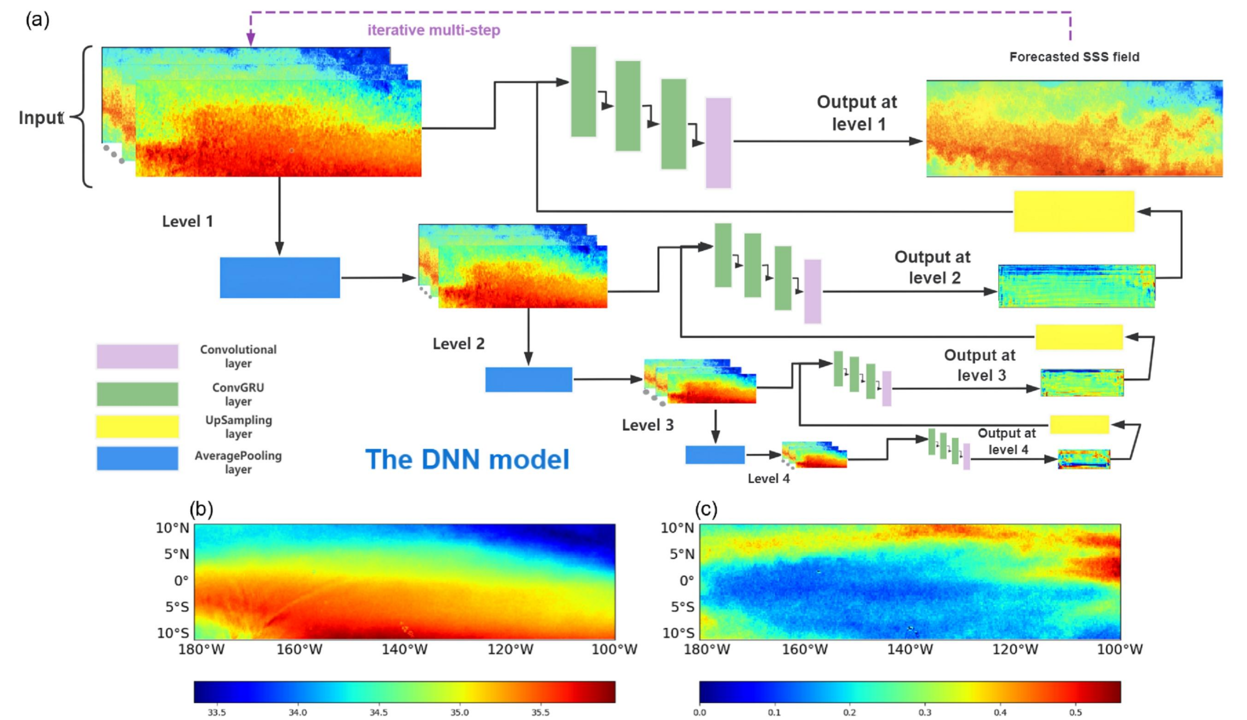

Figure 1. (a) The architecture of the DNN SSS forecast model. The model receives SSS fields at the previous 10 steps and then outputs the SSS at the future time steps. The DNN has four stacked composite layers, each receiving SSS at different resolutions, and has three cascaded ConvGRU layers and one convolutional layer. (b) Mean value and (c) standard deviation of CCI SSS during the testing period.

The Adam (Kingma & Ba et al., 2021) algorithm optimizes DNN parameters with more than 500 epochs to minimize the loss on the training dataset, using a mini-batch size of 64 for each epoch.The learning rate is set to 0.001 at first and then adjusted based on the number of iterations and degree of convergence. The learning rate is reduced by ten with every 200 iterations. The parameters with the smallest loss on the validation dataset are chosen as the final model weight parameters throughout the optimization process. From January 10, 2010, to December 31, 2014, and from January 1, 2015, to December 31, 2019, we divided this period into two non-overlapping periods. Our DNN model was trained using the first five years of data. Then, the performance of our DNN model was tested using the data from the next five years. Since the daily variation of SSS is usually negligible, we set the time step to 6 days and shifted the time series 1 day at a time to build the second, third, fourth, etc., SSS sequence. In each sequence, the SSS from the first 10 steps are fed into the DNN model to forecast the SSS at the next future time step (the 11th step), and the SSS at the 11th step was used as ground truth to evaluate the forecast results of DNN model. During the training and testing periods, we collected 1748 and 1762 samples of SSS sequence, respectively.

3.2 Multi-step ahead forecast

The model used the iterative multi-step (IMS) method (Taieb et al., 2012) after starting with a single-step forecast. . The IMS approach starts with a one-step forecast and then feeds the generated forecast samples to a single-step predictor iteratively to get the next-step forecast. This type of multi-step forecast is simple to use and can recursively generate forecasts of any arbitrary length. For example, the inputs of the previous 10 steps predict the 11th time step, and the SSS forecast was generated at the 12th step using the previous 9 steps and the anticipated time step. Then, iteratively, we made the SSS forecasts at the subsequent time steps (the fourth, fifth, sixth, etc., iterative steps). We varied the forecast lead time from 6 to 96 days (3 months) with the mentioned multi-step forecast approach to the evaluation of El Niño.

3.3 SSS pattern during ENSO events

The propagation direction and dominant speeds of the eastern tropical pacific TIW in the ENSO events were analyzed using the forecast SSS. The difference in dominating propagation rates of TIW can be separate into two periods, centered at 17-and 33-day. To isolate the SSS sequence associated with the TIW, we utilized 28-40-day band-pass filtering (also referred as 33-day) and 13-22-day band-pass (17-day) filtering (Lyman et al., 2007). For further analysis, the TAO SSS and OSTIA SST data are also processed using the same methods. This study used the Niño3.4 SST index method provided by NOAA to calculate the anomalies of the CCI SSS and forecast SSS time series to highlight the features of SSS variations in ENSO events. The SSSA time series is defined as a three-month moving average of average sea surface salinity flattening in the Nino3.4 region (5°S-5°N, 120°W-170°W).

4 Results

4.1 Accuracy

The global salinity of the tropical low salinity zone (170°–100°W, 2°N–10°N) is lower than the salinity value of the south equatorial region (170°–100°W, 0°S–10°S), and the fluctuation range of tropical low salinity zone can approach 0.5 pss, whereas global salinity fluctuation range of the south equatorial region is within 0.1 pss (Figure 1b and 1c). Fresh and saltwater exchange occurs primarily between the equator and extra-equatorial tropical sea in the Pacific Ocean. Similar features appear in the error spatial distribution maps. Forecast errors of the DNN are much smaller than the actual salinity variability in any region.

Compared to actual satellite data and the results of two deep learning models, the DNN model performed well in the subsequent analysis of forecast errors 6 days in advance (Figure S1).

4.2 Iterative forecasting

Our DNN can also work iteratively to predict the SSS sequence of multi-month ahead. For a 3-month lead forecast, we take the SSS predicted by the DNN as the current step (11th step) and combine the previous 9 steps of this step, as an input to predict the SSS of the 12th step. Then, the forecasted SSS of the 12th step with the previous 8 steps can be re-input into DNN to achieve the 13th step (July 24, 2015) lead forecast. This way, we iteratively forecast the SSS sequence from 6 days to 3 months (96 days) lead. Figure 2a and 2b shows a comparison of the average RMSE and MAE forecast by the three models from iterative steps 1 to 16 (i.e., lead time 6 to 96 days). The RMSE of DNN slowly increasing from 0.035 to 0.199 pss, while RMSE of ConvLSTM and ConvGRU increasing sharply from 0.12 to 0.76 pss and 0.12 to 1.16 pss, respectively. The MAE values vary from 0.025 to 0.13 pss, 0.09 to 0.61 pss, and 0.09 to 0.78 pss, respectively. By comparing the results of the three models in three subsequent time steps, the error of ConvLSTM and ConvGRU increases significantly with the emergence of forecast lead time, and the forecast accuracy gradually fails to meet the actual requirements. However, the average RMSE and MAE of DNN are still less than 0.2 pss after 16 iterative steps (as 96 days), with errors increasing slowly. We show the results of the DNN model at the 5th, 10th, and 16th-time steps in Figure S6. Generally, the performance of the DNN is good both in time trends and space.

4.3 SSS pattern in ENSO events

The 33-day filtered satellite SSS variations are consistent with the TAO SSS variations (Figure 2c). The difference between the satellite and TAO SSS values could be partly attributable to the upper ocean's vertical dynamics, 7-day running mean, and data sampling. The forecast SSS and the CCI SSS were used together to analyze the weak La Niña condition in 2016, which caught the propagation of TIWs (Figure 3). The oscillations in the preceding temporal error analysis are consistent with the period when SSSA has large values in the rectangular area and strongly relates to the La Niña event. From August to December 2016, the SSSA was at its peak.

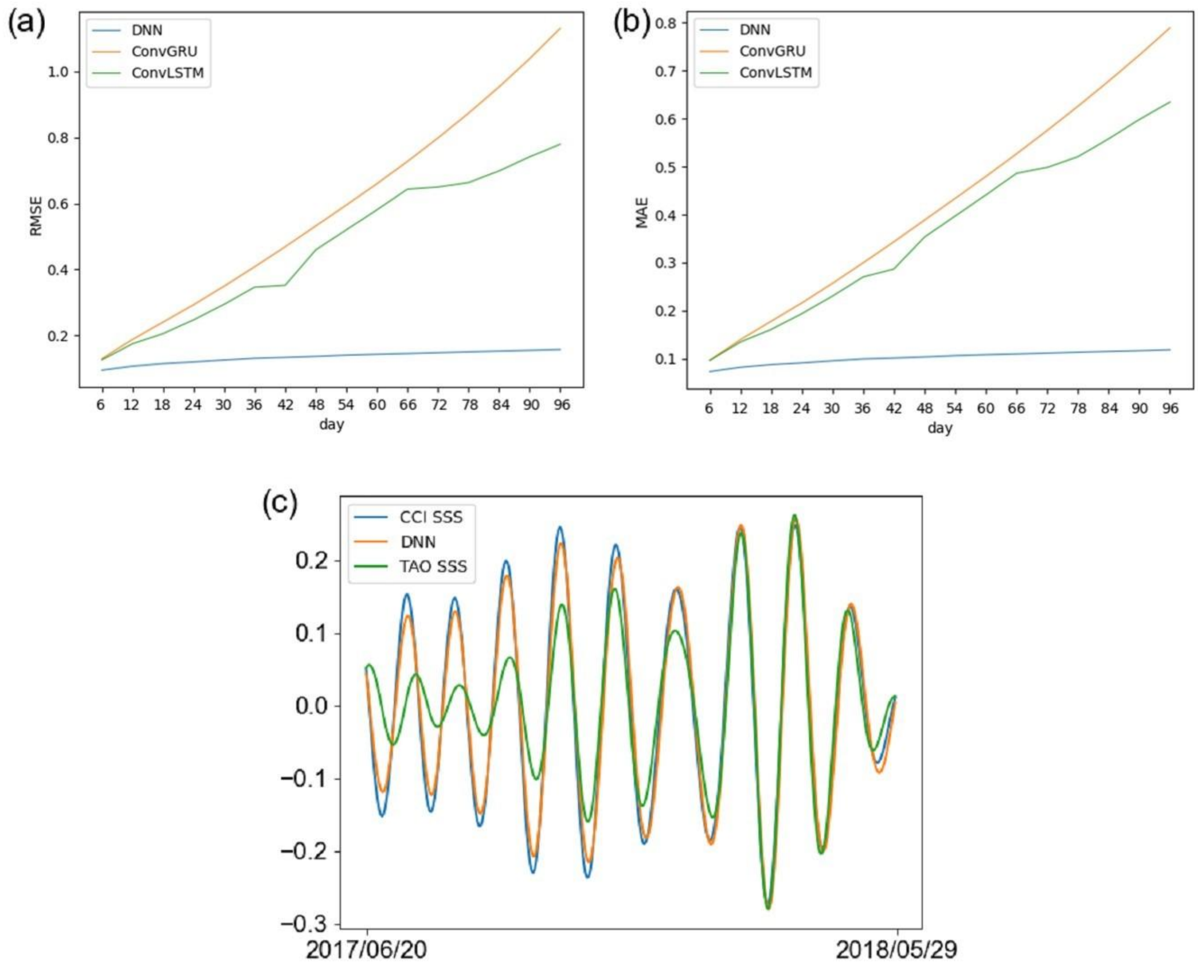

Figure 2. Comparison of time trends of average RMSE and MAE forecast by three deep learning models concerning the number of iterative steps. (a) RMSE and (b) MAE. The iterative steps from 1 to 16 are 6 to 96 days after the previous10 time steps. The DNN model (blue) was compared with the ConvLSTM model (green) and the ConvGRU model (red). (c) CCI SSS (blue line), forecast SSS by DNN (orange line), and TAO SSS (green line) at 110°W and 0°N for the 33-day filtered series from June 2017 to May 2018.

The motion of the SSS pattern westward propagation is evident during the La Niña conditions. However, the non- La Niña condition weakens the SSS pattern of moving westward. Around the west of 110°W, the largest forecast SSS and CCI SSS TIW signals occur. The 33-day filtered CCI SSS and the forecast SSS at 110°W had dominant westward propagation speeds of 1.26m/s. We can see that the CCI and forecast SSS hovmüller diagrams are consistent over the La Niña era. We calculated the bias between the 33-day and 17-day band pass filtered CCI SSS and the SSS forecast by DNN over five years at 110°W bands. The bias of 33-day band pass varies from -0.013 to 0.012 pss, while the bias of 17-day band pass varies from -0.015 to 0.015 pss.

During the strong La Niña period (August to December 2016 and December 2018 to December 2019), the SSSA was roughly 4 months ahead of the SSTA in responding (Figure 3d and 3e), which is similar to the results of several studies compared to the Southern Oscillation Index with a 4-month lag (Delcroix et al.,1998; Chen et al.,2012). Furthermore, SSSA shows a possible dynamic component for a major ENSO event tracer through early SSSA and an early indicator of SSTA in the eastern equatorial Pacific Ocean regions.

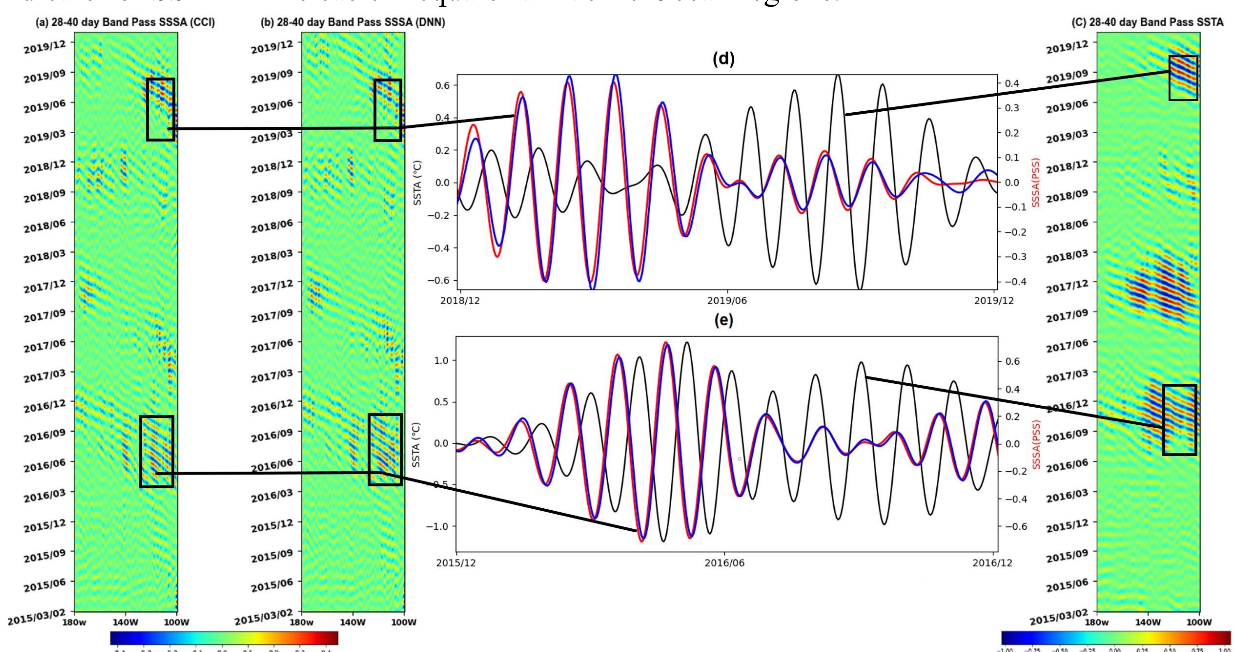

Figure 3. The longitude-time Hovmöller diagram of (a) CCI SSS, (b) forecast SSS (DNN), and (c) OSTIA SST 33-day signals at 5°S bands. (d, e) The filtered CCI SSS signals (red)), filtered forecast SSS (blue), and OSTIA SST signals (black) at 110°W and 5°S for 33-day from December 2015 to December 2016 and December 2018 to December 2019.

The NOAA Climate forecast Center monthly Niño 3.4 SST index data are compared to the monthly time series of SSSA. We also used the daily Niño3.4 SST index data provided by KNMI Climate Explorer to compare with the daily SSSA. SSSA and SSTA showed distinctive features (Figure 4). The Niño 3.4 index shows a strong El Niño extending from April 2015 to March 2016, peaking in December 2015. Weak La Niña conditions also occurred from August to December 2016 (Hackert et al., 2019). The Niño3.4 index values and the forecast time series of SSSA show opposite phases during the strong La Niña period. SST warms/cools dramatically during El Niño/ La Niña periods, and SSS drops/rises sharply. Using the forecast SSS pattern, we can generally distinguish between El Niño (negative anomalies) and La Niña (positive anomalies) events. We compared the monthly, and daily bias for the 6-day and the 96-day SSSA (Figure S8), more than 99% of the absolute bias is less than 0.025.

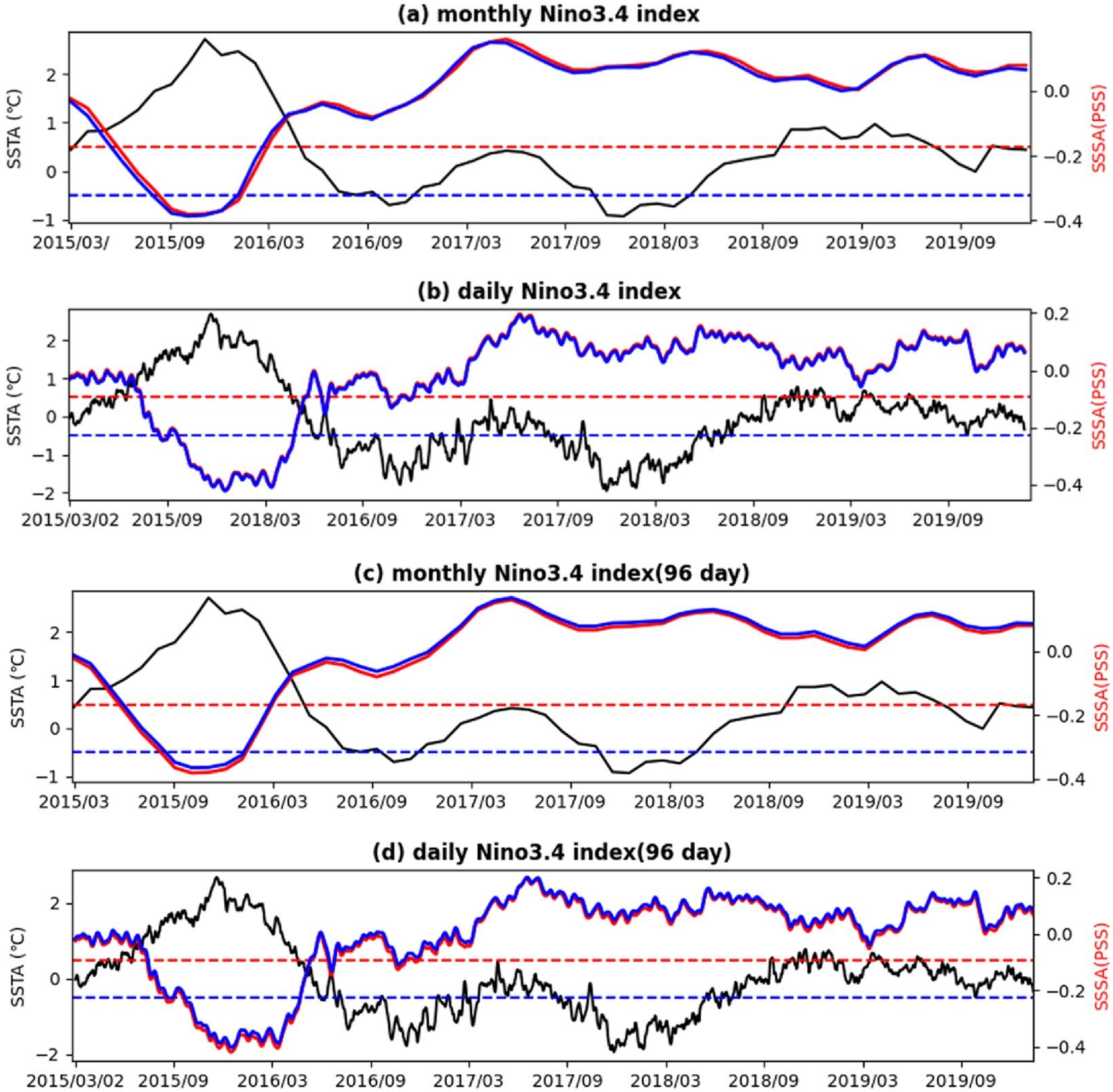

Figure 4. (a-b) Monthly and daily time series of SST anomalies(black), CCI SSS anomalies(red), 6-day DNN forecast SSS anomalies(blue), and (c-d) 96-day DNN forecast results in the Niño 3.4 region (Niño 3.4: 170°–120°W, 5°S–5°N) in 2015–2019, El Niño threshold (red'-') and La Niña threshold (blue'-').

5 Conclusions

Our DNN model can predict SSS fields 6 to 96 days in advance by extracting SSS information from different spatial scales in the tropical Pacific Ocean, which is quite consistent with satellite observations. Since the value of the SSS does not change much throughout the year, the ConvGRU layers used makes it easier to learn how the SSS changes in time while forgetting the unimportant temporal characteristics. Meanwhile the convolutional layers combined with inputs of different spatial scales can better extract spatial information. The forecast errors of SSS are lower than the observed SSS variation over the test period. The forecast error has a fluctuating upward and downward trend with the predicted time series (Figure S4). The forecast

SSS was significant in March 2016 with RMSE and MAE compared to other months. We refer to previous research findings closely related to the 2015-16 Pacific El Niño event (Hackert et al., 2019; Chi et al., 2019). When an event such as ENSO occurs, the SSS forecast will become unstable in a short time series, a part of the model that is difficult to learn but also needs to be overcome.

The anomalies of the forecast SSS over the area 170°–120°W, 5°S–5°N have a strong relationship with the Niño 3.4 SST index. During the strong El Niño event of 2015 - 2016, there was a large variation in SSSA, with the maximum reaching 0.5 pss. From late 2016 to early 2017, the forecast SSSA decreased drastically, closely matching the observed weak La Niña state. Deep learning provides an unprecedented opportunity to forecast the SSS variations associated with TIWs during moderate and non-La Niña periods. The dominant westward propagation speed of SSS reached 1.26m/s from August to December 2016. This oscillation was related to the latitude and dominant period of TIW. The SSS forecast pattern is used to complete the mid-term (3-month) forecast of El Niño and La Niña and is 4 months ahead of SST with consistent performance.

The developed deep learning model is well suited for SSS forecast upto 96 days (about 3 months) in the eastern tropical Pacific Ocean, with RMS less than 0.20. The SSS forecast can be longer than 96 days depending on the tolerance of errors, since the error of the model increase slowly. With only satellite-derived SSS, our DNN can train SSS forecast in a lighter and less time-consuming way than existing models. The SSS forecast the remote sensing CCI SSS data and TAO SSS data are quite consistent.

Ocean satellite remote sensing data and data-driven deep learning technology complement with each other. Deep learning technology extends the usage of ocean satellite data and ocean satellite data enriches the application of deep learning technology. The proposed SSS forecast model supports the forecast of large-scale oceanic and atmospheric phenomena associated with SSS and avoids complicated physical modeling techniques by automatically mining sophisticated principles of SSS spatial-temporal fluctuations associated with El Niño and La Niña events. According to our study, deep learning has a promising future in the SSS pattern forecast of the crucial ocean and climate phenomena. More accurate salinity time series with large-scale spatial coverage and deep learning techniques make SSS-driven ENSO forecast possible.

Acknowledgments

This work was supported by the by the Marine S&T Fund of Shandong Province for Pilot National Laboratory for Marine Science and Technology (Qingdao) (No.2022QNLM050301-1).

Data availability statement

The data used in this study are freely available as follows. CCI SSS datasets are freely available at :

https://catalogue.ceda.ac.uk/uuid/4ce685bff631459fb2a30faa699f3fc5.

OSTIA SST: https://www.ncei.noaa.gov/data/oceans/ghrsst/L4/GLOB/UKMO/OSTIA/.

KNMI Climate Explorer daily Niño3.4 index data : https://climexp.knmi.nl/getindices.cgi?WMO=NCEPData/nino34_daily&STATION=NINO3.4&TYPE=i&id=someone@somewhere&NPERYEAR=366.

NOAA monthly Niño 3.4 SST index data : https://www.cpc.ncep.noaa.gov/data/indices/sstoi.indices.

Data archiving is underway, we temporarily use figshare to store our specific datasets : https://doi.org/10.6084/m9.figshare.20180825.v2.

References

Kido, S., Nonaka, M., & Tanimoto, Y. (2021). Sea surface temperature–salinity covariability and its scale-dependent characteristics. *Geophysical Research Letters*, 48, e2021GL096010. https://doi.org/10.1029/2021GL096010

Lagerloef, G. S. E. (2002). Introduction to the special section: The role of surface salinity on upper ocean dynamics, air-sea interaction and climate. *Journal of Geophysical Research: Oceans*, 107(C12), 8000. doi:10.1029/2002JC001669

Du, Y., Zhang, Y., & Shi, J. (2019). Relationship between sea surface salinity and ocean circulation and climate change. *Science China Earth Sciences*, 62, 771–782. https://doi.org/10.1007/s11430-018-9276-6

Boutin, J., Vergely L., Marchand, S., D'Amico, F., Hasson, A., Kolodziejczyk, N., Reul, N., Reverdin, G., Vialard, J. (2018) New SMOS Sea Surface Salinity with reduced systematic errors and improved variability. *Remote Sensing of Environment*, 214,115-134. https://doi.org/10.1016/j.rse.2018.05.022

Qin, S., Wang, H., Zhu, J. et al. (2020). Validation and correction of sea surface salinity retrieval from SMAP. *Acta Oceanologica Sinica*, 39, 148–158. https://doi.org/10.1007/s13131-020-1533-0

Le Vine, D. M., Lagerloef, G. S. E., Colomb F. R., Yueh S. H., & Pellerano, F. A. Aquarius: An Instrument to Monitor Sea Surface Salinity From Space. *IEEE Transactions on Geoscience and Remote Sensing*, 45, 2040-2050, doi: 10.1109/TGRS.2007.898092

Bao, S., Wang, H., Zhang, R., Yan, H., & Chen, J. (2019). Comparison of satellite-derived sea surface salinity products from SMOS, Aquarius, and SMAP. *Journal of Geophysical Research*: *Oceans*, 124, 1932–1944. https://doi.org/10.1029/2019JC014937

Li, X., Liu, B., Zheng, G., Ren, Y., Zhang, S., Liu, Y., Gao, L., Liu, Y., Zhang, B., & Wang, F. (2020). Deep-learning-based information mining from ocean remote-sensing imagery. *National science review*, 7(10), 1584–1605. https://doi.org/10.1093/nsr/nwaa047

Xiao, C., Chen, N., Hu, C., Wang, K., Gong, J., Chen, Z. (2019). Short and mid-term sea surface temperature prediction using time-series satellite data and LSTM-AdaBoost combination approach. *Remote Sensing of Environment*, 233, 111358. https://doi.org/10.1016/j.rse.2019.111358

Shao, Q., Li, W., Hou, G., Han G., & Wu, X. (2022). Mid-Term Simultaneous Spatiotemporal Prediction of Sea Surface Height Anomaly and Sea Surface Temperature Using Satellite Data in the South China Sea. *IEEE Geoscience and Remote Sensing Letters*, 19, 1-5. doi: 10.1109/LGRS.2020.3042179

Ren,Y., Li, X., & Zhang, W. A data-driven deep learning model for weekly sea ice concentration prediction of the Pan-Arctic during the melting season. *IEEE Transactions on Geoscience and Remote Sensing*. doi: 10.1109/TGRS.2022.3177600.

Ham, YG., Kim, JH. & Luo, JJ. (2019). Deep learning for multi-year ENSO forecasts. *Nature,* 573, 568–572. https://doi.org/10.1038/s41586-019-1559-7

Urquhart, E,A,, Zaitchik, B.F., Hoffman, M.J., Guikema. S.D., Geiger, E.F. Remotely sensed estimates of surface salinity in the Chesapeake Bay: A statistical approach. *Remote Sensing of Environment*, 123, 522-531. DOI: 10.1016/j.rse.2012.04.008

Qing, S., Zhang, J., Cui, T., Bao, Y. (2013). Retrieval of sea surface salinity with MERIS and MODIS data in the Bohai Sea. *Remote Sensing of environment*, 136,117-125. DOI: 10.1016/j.rse.2013.04.016

Song, T., Wang, Z., Xie, P., Han, N., Jiang, J., & Xu, D. (2020). A Novel Dual Path Gated Recurrent Unit Model for Sea Surface Salinity Prediction. *Journal of Atmospheric and Oceanic Technology*, 37(2), 317-325. DOI: https://doi.org/10.1175/JTECH-D-19-0168.1

LeCun, Y., Bengio, Y., & Hinton, G. (2015). Deep learning. *Nature*, 521(7553), 436–444. doi:10.1038/nature14539

Hasson, A., Farrar, J. T., Boutin, J., Bingham, F., & Lee, T. (2019). Intraseasonal variability of surface salinity in the eastern tropical Pacific associated with mesoscale eddies. *Journal of Geophysical Research: Oceans*, 124, 2861– 2875. https://doi.org/10.1029/2018JC014175

Kolodziejczyk, N., Hamon, M., Boutin, J., Vergely, J., Reverdin, G., Supply, A., & Reul, N. (2021). Objective Analysis of SMOS and SMAP Sea Surface Salinity to Reduce Large-Scale and Time-Dependent Biases from Low to High Latitudes. *Journal of Atmospheric and Oceanic Technology,* 38(3), 405-421. doi:10.1175/jtech-d-20-0093.1

Huang, M., Liang, X., Zhu, Y., Liu, Y., & Weisberg, R. H. (2021). Eddies connect the tropical Atlantic Ocean and the Gulf of Mexico. *Geophysical Research Letters*, 48, e2020GL091277. https://doi.org/10.1029/2020GL091277

Lin, X., Q., Y.; Sun, D. (2019). Thermohaline Structures and Heat/Freshwater Transports of Mesoscale Eddies in the Bay of Bengal Observed by Argo and Satellite Data. *Remote Sensing*, 11,2989. doi:https://doi.org/10.3390/rs11242989

Melnichenko, O., Hacker, P., Müller, V. (2021). Observations of Mesoscale Eddies in Satellite SSS and Inferred Eddy Salt Transport. Remote Sensing,13(2):315. https://doi.org/10.3390/rs13020315

Shi, X., et al. (2015).Convolutional LSTM Network: A Machine Learning Approach for Precipitation Nowcasting. *neural information processing systems,* 1-12. doi: https://doi.org/10.48550/arXiv.1506.04214

Ma, T., Zhang, L., Diao, X., Ma, O. (2020). ConvGRU in Fine-grained Pitching Action Recognition for Action Outcome forecast. *ArXiv*. https://doi.org/10.48550/arXiv.2008.07819

Boutin, J., Reul, N., Koehler, J., Martin, A., Catany, R., Guimbard, S., et al. (2021). Satellite-based sea surface salinity designed for ocean and climate studies. *Journal of Geophysical Research: Oceans,* 126, e2021JC017676. https://doi.org/10.1029/2021JC017676

Zheng, G., Li, X., Zhang, R., Liu, B. (2021). Purely satellite data–driven deep learning forecast of complicated tropical instability waves. Science Advances, 6, 29. https://doi.org/10.1126/sciadv.aba1482

Krizhevsky, A., Sutskever, I. & Hinton, G. E. (2012). Imagenet classifcation with deep convolutional neural networks. Communications of the ACM, 60, 84 – 90. https://doi.org/10.1145/3065386

Nair, V., & Hinton, G.E. (2010). Rectified Linear Units Improve Restricted Boltzmann Machines. *in International Conference on International Conference on Machine Learning,* Madison, WI, USA,807–814.

Kingma, D. P., & Ba, J. (2017). Adam: A method for stochastic optimization, *in International Conference on Learning Representations 2015*, San Diego, CA, 7 to 9 May 2015. https://doi.org/10.48550/arXiv.1412.6980

Taieb, S. B., Bontempi, G., Atiya, A. F., Sorjamaa, A. (2012). A review and comparison of strategies for multi-step ahead time series forecasting based on the NN5 forecasting competition. *Expert Systems with Applications*, 39, 7067-7083. https://doi.org/10.1016/j.eswa.2012.01.039

Lyman, J.M., Johnson, G.C., Kessler, S. (2007). Distinct 17- and 33-day tropical instability waves in subsurface observations. *Journal of Geophysical Research: Oceans*. 37, 855–872. doi: https://doi.org/10.1175/JPO3023.1

Delcroix, T. (1998). Observed surface oceanic and atmospheric variability in the tropical Pacific at seasonal and ENSO timescales: A tentative overview. *Journal of Geophysical Research: Oceans*, 103(C9), 18611– 18633, doi:10.1029/98JC00814.

Chen, J., Zhang, R., Wang, H. et al. (2012). Isolation of sea surface salinity maps on various timescales in the tropical Pacific Ocean. *Journal of Oceanography*, 68, 687–701 https://doi.org/10.1007/s10872-012-0126-8

Hackert, E. C., Kovach, R. M., Busalacchi, A. J., Ballabrera-Poy, J. (2019). Impact of Aquarius and SMAP satellite sea surface salinity observations on coupled El Nino/Southern Oscillation forecasts. *Journal of Geophysical Research: Oceans*, 124, 4546–4556, doi: https://doi.org/10.1029/2019JC015130

Chi, J., Du, Y., Zhang, Y., et al. (2019) A new perspective of the 2014/15 failed El Niño as seen from ocean salinity. *Scientific Reports*, 9, 2720. https://doi.org/10.1038/s41598-019-38743-z